

# Regulation of membrane scission in yeast endocytosis

Deepikaa Menon<sup>1</sup> and Marko Kaksonen<sup>1\*</sup>

\*For correspondence:  
Marko.Kaksonen@unige.ch

<sup>1</sup>Department of Biochemistry, University of Geneva, Geneva, Switzerland

## Abstract

### Introduction

Clathrin-mediated endocytosis (CME) is an endocytic process by which cargo from the cell exterior is incorporated into a Clathrin-coated vesicle that is then transported into the cell (*Bitsikas et al., 2014*). Over 50 different proteins are involved in reshaping a flat plasma membrane into an invagination that eventually separates from the plasma membrane to form a vesicle (*Kaksonen and Roux, 2018*). In yeast, CME is the only pathway for uptake of cargo, and involves a similar membrane transformation as in other eukaryotes. Most mammalian CME proteins have homologues in yeast: these proteins drive the establishment of endocytic sites, and form the mechanical link between membrane and actin proteins (*Kaksonen and Roux, 2018*). Actin nucleation and polymerization produces the forces that form tubular invaginations in yeast (*Kübler et al., 1993; Kaksonen et al., 2003*). Forces that drive the final transition from tubular invagination to spherical vesicle in multicellular eukaryotes are provided by the GTPase Dynamin (*Grigliatti et al., 1973; Sweitzer and Hinshaw, 1998; Ferguson et al., 2007; Takei et al., 1995; Galli et al., 2017*). Dynamin is now known to interact via its proline-rich-domain with the SH3 domains of crescent-shaped N-BAR proteins like Endophilin and Amphiphysin (*Grabs et al., 1997; Cestra et al., 1999; Farsad et al., 2001; Ferguson et al., 2009; Meinecke et al., 2013*). Conformation changes of Dynamin recruited to N-BAR molecules cause constriction of the underlying invaginated membrane, resulting in vesicle formation (*Shupliakov et al., 1997; Zhang and Hinshaw, 2001; Zhao et al., 2016*).

The role of Dynamin in yeast endocytosis has been debated: yeast dynamin-like protein Vps1 has a major role in the Golgi and other membrane trafficking pathways (*Rothman et al., 1990; Peters et al., 2004; Hoepfner et al., 2001*), and been proposed to interact with endocytic proteins (*Nannapaneni et al., 2010; Yu and Cai, 2004; Smaczynska-de Rooij et al., 2012*). Its contribution to CME is however, still debated (*Goud Gadila et al., 2017; Kishimoto et al., 2011*). In yeast cells, what causes membrane scission is thus unclear, although the yeast N-BAR Rvs complex (a heterodimeric complex of the proteins Rvs161 and Rvs167) has been identified as an important component of the scission module (*Munn et al., 1995; Kaksonen et al., 2005; D'Hondt et al., 2000; Kishimoto et al., 2011*). The two Rvs proteins are homologues of N-BAR proteins Amphiphysin and Endophilin (*Friesen et al., 2006; Youn et al., 2010*). Deletion of Rvs167 reduces scission efficiency by nearly 30% and reduces the invagination lengths at which scission occurs (*Kaksonen et al., 2005; Kukulski et al., 2012*). Apart from the canonical N-BAR domain which forms the crescent-shaped structure, Rvs167 has a Glycine-Proline-Alanine rich (GPA) region and a C-terminal SH3 domain (*Sivadon et al., 1997*). The GPA region is thought to act as a linker with no other known function, while loss of the SH3 domain affects budding pattern and actin morphology (*Sivadon et al., 1997*). Most Rvs

43 deletion phenotypes can be rescued by expression of the BAR domains alone (*Sivadon et al., 1997*),  
44 suggesting that the BAR domains are the functional unit of the Rvs complex.

45 The Rvs complex can tubulate liposomes in vitro, indicating that the BAR domains can impose  
46 curvature on membranes (*Youn et al., 2010*). However, Rvs arrives at endocytic sites when mem-  
47 brane tubes are already formed: curvature sensing rather than generation is the likely interaction  
48 of the complex with endocytic sites (*Kukulski et al., 2012; Picco et al., 2015*). Rvs molecules arrive  
49 at endocytic sites about 4 seconds before scission, and disassemble rapidly at the time of scission  
50 (*Picco et al., 2015*), consistent with a role in scission. While it is shown to be involved in the last  
51 stages of endocytosis, a mechanistic understanding of the influence of Rvs on scission remains  
52 incomplete.

53  
54 Several scission models have been proposed that allow a major role for Rvs and are tested in  
55 this work. Although the yeast Dynamin Vps1 lacks a canonical BAR-protein binding site (*Bui et al.,*  
56 *2012; Moustaq et al., 2016*), it may be recruited via a different mechanism and induce scission.  
57 Liu et al., proposed that Synaptojanins may selectively hydrolyze lipids at endocytic sites, causing  
58 line tension between two lipid types that results in scission (*Liu et al., 2009*). Protein friction  
59 along the membrane invagination has been proposed as a mechanism by which scission may  
60 occur (*Simunovic et al., 2017*). We used quantitative live-cell imaging and genetic manipulation in  
61 *Saccharomyces cerevisiae* to test these theories and investigate the function of Rvs in endocytosis.  
62 We found that Rvs is recruited to endocytic sites by both BAR and SH3 domains. Of several potential  
63 actin-interacting binding partners of the SH3 domains such as Myo3, Myo5, Vrp1, Abp1 (*Lila and*  
64 *Drubin, 1997; Colwill et al., 1999; Madania et al., 1999; Liu et al., 2009*), we found that type I myosin  
65 Myo3 interacts with Rvs SH3 domains. Our data also suggests that the aforementioned theories  
66 of membrane scission are unlikely to sever the membrane in yeast, and that actin polymerization  
67 likely generates the forces required for scission.

## 68 Results

### 69 **Rvs167, rather than Vps1 influences coat movement**

70 Yeast Dynamin-like protein Vps1 does not contain a Proline Rich Domain, which in mammalian  
71 cells is required for recruitment to endocytic sites (*Grabs et al., 1997; Cestra et al., 1999; Farsad*  
72 *et al., 2001; Meinecke et al., 2013*). In spite of the lack of a stereotypical interaction domain, some  
73 works have reported its recruitment to endocytic proteins, including to N-BAR protein Rvs167 (*Yu*  
74 *and Cai, 2004; Nannapaneni et al., 2010; Rooij et al., 2010*). The question of whether or not Vps1  
75 has a function at endocytic sites has been obfuscated by potential tagging-induced dysfunction  
76 of Vps1 molecules. Vps1 tagged both N- and C-terminally with GFP constructs failed to co-localize  
77 with endocytic protein Abp1 in our hands, consistent with other work that observed localization  
78 only with other parts of the trafficking pathway (*Goud Gadila et al., 2017*). We argued that even  
79 if tagging Vps1 induced defects in its localization and/or function, its contribution to endocytosis  
80 could be examined by observing the dynamics of other endocytic proteins in cells lacking Vps1. The  
81 canonical interaction partner of Vps1- Rvs167- localizes to endocytic sites, and has a role in scission,  
82 although it is unclear what that is (*Kukulski et al., 2012; Picco et al., 2015*). In order to determine  
83 the roles of these proteins in endocytic scission, we studied cells lacking Vps1 and Rvs167, and  
84 compared against wild-type (WT) cells (Fig.1A-F).

85  
86 Vps1 deletion was confirmed by sequencing the gene locus, and these cells showed a previously  
87 reported (*Rothman and Stevens, 1986*) growth phenotype at high temperatures (Fig.S1). Scission  
88 efficiency was quantified by tracking the endocytic coat protein Sla1 tagged at the C-terminus with  
89 eGFP (Fig.1C). Upon actin polymerization, the endocytic coat moves into the cytoplasm along with  
90 the membrane as it invaginates (*Skrzyny et al., 2012*). Movement of coat protein Sla1 thus acts as a  
91 proxy for the growth of the plasma membrane invagination. Membrane retraction, that is, inward

92 movement and subsequent retraction of the invaginated membrane back towards the cell wall is a  
 93 scission-specific phenotype (*Kaksonen et al., 2005*). Retraction rates do not significantly increase in  
 94 *vps1Δ* cells compared to the WT (Fig.1C).

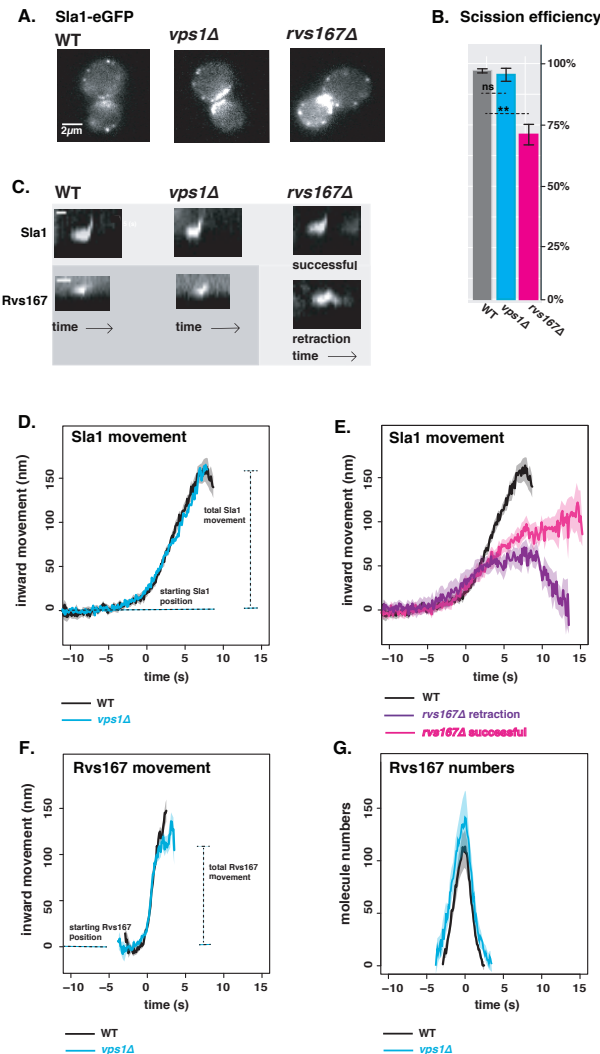


**Figure 1. *vps1Δ* and *rvs167Δ* deletion** **A:** Single slices from time lapse movies of WT, *vps1Δ*, and *rvs167Δ* cells expressing Sla1-eGFP. Scale bar = 2μm. **B:** Representative kymographs of Sla1-eGFP and Rvs167-eGFP patches in WT, *vps1Δ*, and *rvs167Δ* cells from time lapse movies. Scale bar for Sla1-egfp = 20(s), scale bar for Rvs167-eGFP = 5(s). **C:** Scission efficiency in WT, *vps1Δ*, and *rvs167Δ* cells. Error bars are standard deviation, p values from t-test, \* = p ≤ 0.05, \*\* = p ≤ 0.01, \*\*\* = p ≤ 0.001. **D:** Averaged centroid positions of Sla1-eGFP in WT and *vps1Δ* cells. **E:** Averaged position of Rvs167-eGFP in WT and *vps1Δ* cells. **F:** Averaged position of Sla1-eGFP in WT, and successful and retracted Sla1-eGFP positions in *rvs167Δ* cells. All averaged positions were aligned in x axis to begin inward movement at time=0(s), and aligned in the y axis to a starting position = 0(nm).

95  
 96 The total movement of the endocytic coat (Fig.1D,E) gives an indication of when invagination has  
 97 undergone scission: greater movement would imply defects in the scission mechanism. In order  
 98 to study this movement, the averaged centroid trajectory of 50 Sla1-eGFP patches in *vps1Δ* and  
 99 WT cells were tracked and compared (Fig.1D). In brief: yeast cells expressing fluorescently-tagged  
 100 endocytic proteins were imaged at the equatorial plane. Since membrane invagination progresses  
 101 perpendicularly to the plane of the plasma membrane, proteins that move into the cytoplasm

102 during invagination do so in the imaging plane. Centroids of Sla1 patches- each patch being an  
103 endocytic site- were tracked in time and averaged. This provided an average centroid that could be  
104 followed with high spatial and temporal precision (*Picco et al., 2015*). Averaged centroid movement  
105 of Sla1-eGFP in WT cells was linear to about 140nm (Fig.1D). Sla1 movement in *vps1Δ* cells had the  
106 same magnitude of movement (Fig.1D). In spite of slight differences in the rates of movement, the  
107 total movement- and so the depth of endocytic invagination- did not change.  
108  
109 Centroid tracking has shown that the number of molecules of Rvs167 peaks at the time of scission,  
110 and is followed by a rapid loss of fluorescent intensity, simultaneous with a sharp jump of the  
111 centroid into the cytoplasm (*Picco et al., 2015*). This jump, also seen in Rvs167-GFP kymographs  
112 (Fig.1B), is interpreted as loss of protein on the membrane tube, causing an apparent spatial jump  
113 to the protein localized at the base of the newly formed vesicle. Kymographs of Rvs167-GFP (Fig.1B),  
114 as well as Rvs167 centroid tracking (Fig.1E) in Vps1 deleted cells showed the same jump as in WT.  
115  
116 The Rvs complex is composed of Rvs161 and Rvs167 dimers (Boeke et al. 2014) so deletion of  
117 Rvs167 effectively removes both proteins from endocytic sites. We quantified the effect of *rvs167Δ*  
118 on membrane invagination (Fig.1A-C,F). Only 73% of Sla1 patches undergo successful scission in  
119 *rvs167Δ* cells (Fig.1C). Similar scission rates have been measured in other experiments (*Kaksonen*  
120 *et al., 2005*), and suggest failed scission in the remaining 27% of endocytic events. Coat movement  
121 both of retractions and of successful endocytic events were quantified (Fig.1F) as described earlier.  
122 Sla1 centroid movement in both successful and retracting endocytic events in *rvs167Δ* cells look  
123 similar to WT up to about 50nm (Fig.1F). In WT cells, Abp1 intensity begins to drop at scission  
124 time (Fig.S2); similarly, in successful endocytic events, Abp1 intensity drops after Sla1 centroid has  
125 moved about 100nm suggesting that scission occurs at invagination lengths between 60 -100 nm  
126 (Fig.S4). That membrane scission occurs at shorter invagination lengths than in WT is corroborated  
127 by the smaller vesicles formed in *rvs167Δ* cells by Correlative light and electron microscopy (CLEM)  
128 (*Kukulski et al., 2012*). CLEM has moreover shown that Rvs167 localizes to endocytic sites after  
129 the invaginations are about 60nm long (*Kukulski et al., 2012*). Sla1 movement in *rvs167Δ* indicates  
130 therefore that membrane invagination is unaffected till Rvs is supposed to arrive.

131 **Synaptojanins likely influence vesicle uncoating, but not scission dynamics.**  
132 As Vps1 did not appear to influence membrane scission, we proceeded to test another scission  
133 model. The lipid hydrolysis model proposes that deletion of yeast synaptojanins would inhibit  
134 scission and therefore result in longer invaginations (*Liu et al., 2009*). Three Synaptojanin-like  
135 proteins have been identified in *S. cerevisiae*: Inp51, Inp52, and Inp53. Inp51-eGFP exhibits a  
136 diffuse cytoplasmic signal, Inp52-eGFP localizes to cortical patches that are endocytic sites (Fig.2A,  
137 supplement) and Inp53 localizes to patches within the cytoplasm (Fig.2A, (*Bensen et al., 2000*)). Since  
138 Inp52 localizes to endocytic sites, we began with determining the spatial and temporal recruitment  
139 of Inp52 within the endocytic machinery. We aligned the averaged centroid of Inp52 in space and  
140 time to other endocytic proteins (*Picco et al., 2015*). In order to do this, we imaged Inp52-eGFP  
141 simultaneously with Abp1-mCherry, and did the same with Sla1-eGFP and Rvs167-eGFP. Using Abp1  
142 as the common reference frame, we were able to compare the arrival of the different proteins with  
143 respect to that of Abp1. We assigned as time =0 (s) the fluorescent intensity maximum of Abp1,  
144 which in WT cells is concomitant with membrane scission, and also coincides with the maximum  
145 of the Rvs167 fluorescent intensity (Fig.1A, S3). On the y axis, 0 (nm) indicates the position of the  
146 Sla1 centroid; positions of the other centroids are in relation to the Sla1 centroid. Inp52 molecules  
147 arrived in the late stage of endocytosis after Rvs167 arrival, and localized to the invagination tip,  
148 suggesting a potential role in membrane scission (Fig.2B).

149 Inp53 was not investigated further, as its localization conformed with other literature that found  
150 that it is involved in the golgi trafficking pathway and not endocytosis (*Bensen et al., 2000*). Although  
151 we were unable to observe localization of Inp51 at endocytic sites, deletion of Inp51 has been

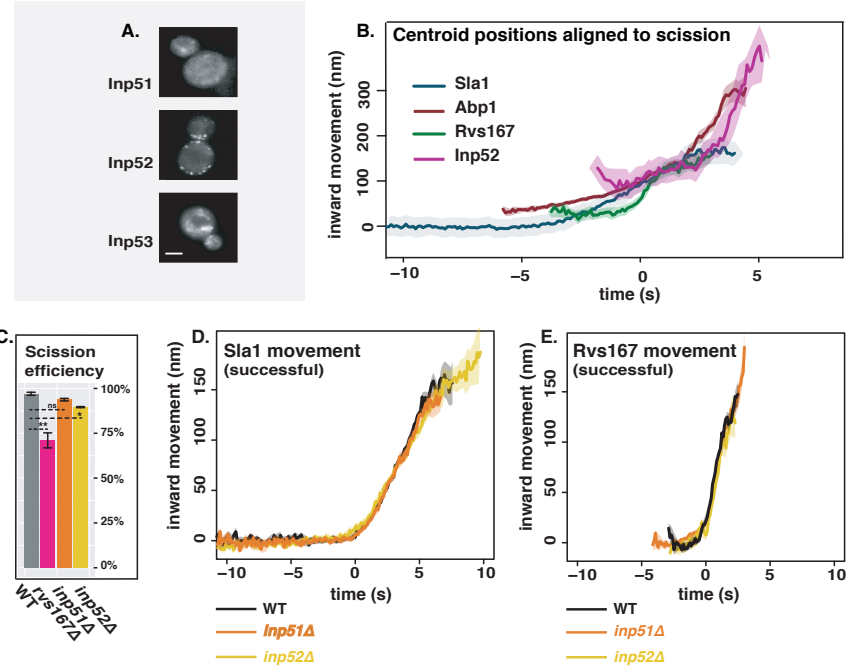


**Figure 2. Involvement of yeast Synaptojanin-like proteins in endocytosis** **A:** Cells endogenously tagged with Inp51-, Inp52-, and Inp53-eGFP. **B:** Inp52 centroid trajectory was aligned in space and time to other endocytic proteins. **C:** Sla1 retraction rates in *inp51Δ* and *inp52Δ* cells compared to WT and *rvs167Δ*. Error bars are standard deviation, with p values from t-test, \* =  $p \leq 0.05$ , \*\* =  $p \leq 0.01$ , \*\*\* =  $p \leq 0.001$ . **D:** Averaged centroid positions of Sla1-eGFP in WT, *inp51Δ*, and *inp52Δ* cells. **E:** Averaged centroid positions of Rvs167-eGFP in WT, *inp51Δ*, and *inp52Δ* cells.

152 shown to exacerbate the effect of *inp52Δ* on membrane retraction (*Liu et al., 2009*), so both Inp51  
153 and Inp52 were tested as potential scission regulators.

154

155

156 Dynamics of Sla1-eGFP and Rvs167-eGFP in *inp51Δ* and *inp52Δ* cells were compared against  
157 the WT (Fig.2C-E). Scission efficiency did not significantly decrease in *inp51Δ* compared to the WT,  
158 but showed a slight decrease in *inp52Δ* cells (Fig2C). Total movement of Sla1 and Rvs167 centroids  
159 in *inp51Δ* were the same as in WT (Fig.2 D,E), while Rvs167 assembly and disassembly took longer  
160 (Fig.S5). Rvs167 centroid, after the inward movement, appeared to persist compared to the WT,  
161 likely because of a delay in Rvs167 disassembly from the newly formed vesicle. In *inp52Δ* cells,  
162 Sla1 movement had the same magnitude and rate as in WT, but Sla1-eGFP signal is persistent after  
163 inward movement scission (Fig.2D). Rvs167 and Sla1 disassembly were delayed in *inp52Δ* cells  
164 compared to WT (Fig.2supplement1). This data are consistent with Synaptojanin involvement in  
165 assembly and disassembly of coat and scission proteins at endocytic sites rather than in membrane  
166 scission.

167

#### Rvs BAR domains recognize membrane curvature in-vivo

168 So far Rvs167 remains the protein that has a major influence on scission efficiency and movement  
169 of Sla1. Rvs can tubulate liposomes in vitro (*Youen et al., 2010*), but its interaction with membrane  
170 curvature in vivo has not so far been tested. Recruitment of the Rvs complex to endocytic sites, and  
171 BAR-membrane interaction was thus investigated further. The SH3 domain has known interactions  
172 with proteins within actin network (*Lila and Drubin, 1997; Colwill et al., 1999; Madania et al., 1999;*  
173 *Liu et al., 2009*). We removed the contribution of the SH3 by deleting the domain (Fig.3A) and  
174 observed the localization of Rvs167 $\Delta$ sh3 compared to full-length Rvs167. Endogenously tagged

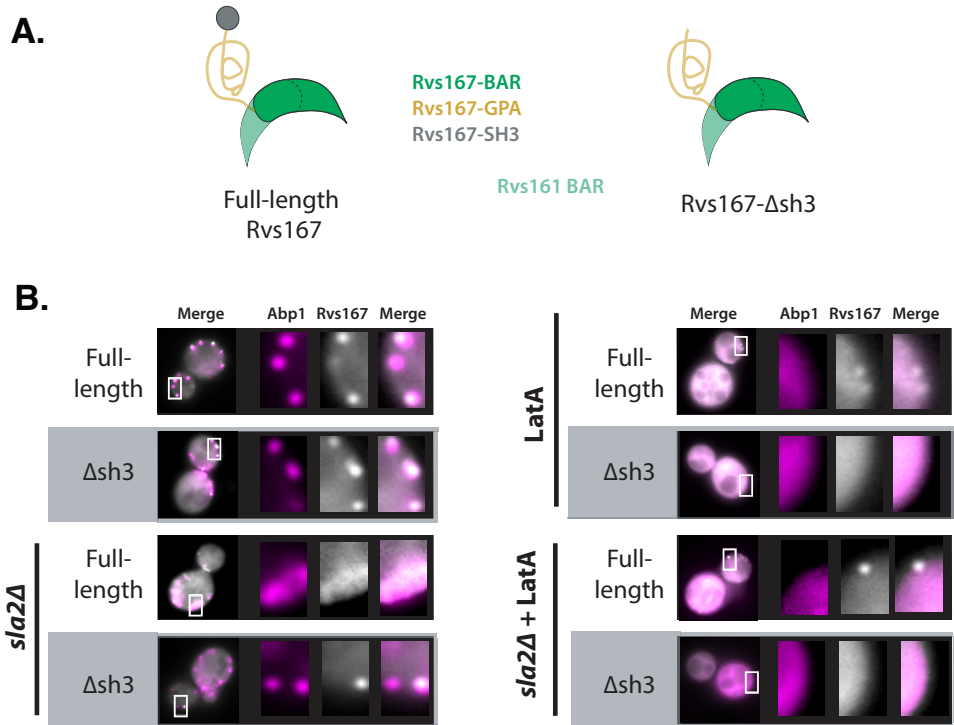


**Figure 3. Localization of Rvs167 BAR domain** **A:** Schematic of Rvs protein complex with and without the SH3 domain. **B:** Localization of full-length Rvs167 and Rvs167 $\Delta$ sh3 in WT, *sла2Δ*, LatA treated, and LatA treated *sла2Δ* cells. Scale bar=2 $\mu$ m.

Rvs167-eGFP and Rvs167 $\Delta$ sh3-eGFP colocalization with Abp1-mCherry in WT and *sла2Δ* cells were compared (Fig.3B). Sla2 acts as the molecular linker between forces exerted by the actin network and the plasma membrane (*Skruzny et al., 2012*). *sла2Δ* cells therefore contain a polymerizing actin network at endocytic patches, but the membrane has no curvature, and endocytosis fails. In these cells, the full-length Rvs167 co-localizes with Abp1-mCherry, indicating that it is recruited to endocytic sites independently of membrane curvature (Fig.3B, “*sла2Δ*”). Rvs167 $\Delta$ sh3 does not localize to the plasma membrane except for rare transient patches that do not co-localize with Abp1-mCherry: Rvs167 $\Delta$ sh3 is not recruited to endocytic sites in the absence of curvature in *sла2Δ* cells.

#### 184      **Rvs SH3 domains have an actin and curvature independent localisation**

In order to test if genetic interactions of SH3 domains are prevalent in *in vivo* endocytosis, we tested the localization of Rvs167 and Rvs167 $\text{texit}\Delta$ sh3 in LatA treated cells (Fig.3B, “LatA”). Plasma membrane localization of Rvs167 remains upon LatA treatment, and transient patches continue to exist in *sла2Δ* cells treated with LatA (Fig3B, “*sла2Δ+ LatA*”). Rvs167 $\text{texit}\Delta$ sh3 does not localize to the plasma membrane in either case. Thus, localization of full-length Rvs167 in the presence of LatA is due to the SH3 domain. This indicates that the SH3 domain is able to recruit Rvs molecules to the plasma membrane in an actin- and curvature-independent manner.

#### 192      **SH3 domains are likely recruited by Myosin 3**

Type I myosins Myo3 and Myo5, and Vrp1 have known genetic and/or physical interactions with Rvs167 SH3 domains (*Lila and Drubin, 1997; Colwill et al., 1999; Madania et al., 1999; Liu et al., 2009*). We tested the interaction between these proteins and the Rvs167 SH3 region by studying the localization of full-length Rvs167 in cells with one of the genes for these proteins deleted, and

treated with LatA. By using LatA we expected to reproduce the situation in which BAR-curvature interaction is removed (Fig.4B). Then, if we lost SH3 interaction because we removed the protein with which it interacts, we would lose localization of Rvs167 completely. Deletion of neither Vrp1 nor Myo5 in combination with LatA treatment removes the localization of Rvs167. Deletion of Myo3 with LatA treatment removes localization of Rvs167, indicating that SH3 domains interact at endocytic sites with Myo3.

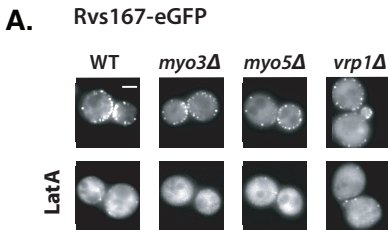


**Figure 4. Localization of the SH3 domain** Localization of full-length Rvs167-eGFP in WT, *myo3Δ*, *myo5Δ*, and *vrp1Δ* cells. Scale bars=2μm.

what about the differences in *myo5* and *myo3* number...

#### Loss of Rvs167 SH3 domain affects coat and actin dynamics

Since the Rvs167 SH3 domain has an influence on the recruitment of the Rvs complex to endocytic sites, we wondered if the domain also affects later stages of invagination formation endocytic dynamics. We compared dynamics of coat and scission markers in WT and *rvs167Δsh3* cells (Fig.5). Movement of Sla1 centroid is slower and reduced in *rvs167Δsh3* cells compared to WT (Fig4A,B). The movement of Rvs167textitΔsh3 centroid is smaller than that of full-length Rvs167 (Fig.5A,B), consistent with the formation of shorter invaginations suggested by the reduced Sla1 movement in *rvs167Δsh3* cells.

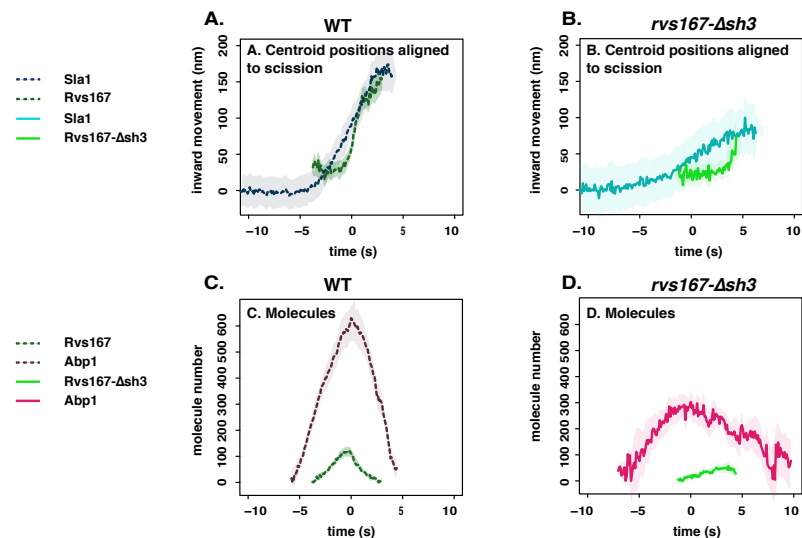


**Figure 5. Endocytic dynamics in *rvs167Δsh3* cells** **A,B:** Averaged centroid positions aligned in x axis so that time=0(s) is the peak of fluorescent intensity of Abp1 in respective strains. Centroids are aligned in y axis so that Sla1 begins at y=0 (nm), and Rvs167 and Rvs167-Δsh3 positions are determined with respect to Sla1 centroids. **C,D:** Numbers of molecules in WT and *rvs167Δsh3* cells, aligned so that time=0(s) is the maximum of fluorescent intensity of Abp1 in the corresponding strains.

212 There is delay in Rvs167 $\Delta$ sh3 recruitment compared to the onset of Abp1 assembly in *rvs167 $\Delta$ sh3*  
213 cells compared to WT (Fig.5 C,D). In WT cells, Rvs167 and Abp1 molecule number peaks are also co-  
214 incident: the actin network begins disassembling as soon as scission occurs (Fig.5C). Asynchronous  
215 peaks in *rvs167 $\Delta$ sh3* cells indicates a disruption in the feedback between actin network dynamics  
216 and membrane scission. Rvs167textit $\Delta$ sh3 accumulation begins however, when Abp1 molecule  
217 numbers in the mutant are about the same as in WT (about 300 copies, Fig.5C,D). . Both Rvs167  
218 and Rvs167 $\Delta$ sh3 molecules arrive at endocytic sites when the Sla1 centroid is 20-30 nm away from  
219 its starting position. This would mean the endocytic coat has moved about 30 nm when both WT  
220 and mutant forms of Rvs are recruited. That Rvs167 $\Delta$ sh3 recruitment anticipates a certain growth  
221 of the invagination and amount of Abp1 suggests that the Rvs complex is recruited to a specific  
222 geometry of membrane invagination, and that Rvs167 $\Delta$ sh3 recruitment is delayed because invagi-  
223 nations in these cells take longer to acquire this specific geometry. Recruitment of Rvs167 $\Delta$ sh3 is  
224 reduced to half of Rvs167 (Fig.5C,D), although cytoplasmic concentration of both are similar (Fig.S6).  
225 Recruitment therefore is unlikely to be limited by cytoplasmic expression of the mutant protein.  
226 Abp1 disassembly is slowed down in *rvs167 $\Delta$ sh3* cells compared to WT, and recruitment is reduced  
227 to 50% of WT recruitment (Fig.5C,D), indicating disruption of actin network dynamics.

228 **Increased BAR domain recruitment corresponds to increased membrane move-  
229 ment**

230 Since removal of Rvs167 in *rvs167 $\Delta$ sh3* cells, and the reduced amount of Rvs167 $\Delta$ sh3 recruited in  
231 *rvs167 $\Delta$ sh3* cells results in decreased Sla1 movement, we wondered if Sla1 movement would scale  
232 with amount of Rvs recruited to endocytic sites. We titrated the amount of Rvs expressed in cells by  
233 endogenously duplicating the Rvs167 and Rvs161 genes (Huber et al. 2014) in diploid and haploid  
234 yeast cells (Fig.5) . We thus made diploid strains with 4x copies of both the Rvs genes (4xRVS), 2x  
235 copies (WT diploid cells, 2xRVS), and 1x copy (1xRVS). Number of molecules of Rvs167 recruited  
236 to endocytic sites increases with gene copy number (Fig5A). "Excess" Rvs recruited to endocytic  
237 sites in the 4xRVS case does not change the rate or total movement of Sla1, or of Rvs167 (Fig.6B,C)  
238 compared to the WT (2xRVS). In the case of 1xRVS, Sla1 movement is slightly reduced after 100nm  
239 (Fig.6B). Magnitude of Rvs167 inward movement was similar in all three, but the Rvs167-eGFP signal  
240 was lost immediately after the inward movement in the 1xRVS case, unlike in the 4xRVS and 2xRVS  
241 cases, likely because fewer molecules are recruited (Fig.6A). Unlike in the *rvs167 $\Delta$ sh3* case, Abp1  
242 and Rvs167 peaks were concomitant in all three strains, with similar amounts of Abp1 recruited  
243 irrespective of Rvs gene copies (Fig.6D). Thus was there no apparent disruption of the actin network,  
244 or of the coupling between scission and actin network disassembly. Adding more Rvs than in the  
245 WT diploid case did not lead to differences in Sla1 movement, although reducing the amount of Rvs-  
246 as in the 1xRVS case- marginally decreased movement.

247 In haploid cells, we duplicated the full-length Rvs167 gene, as well as *rvs167 $\Delta$ sh3* gene (Fig5E-H).  
248 We thus produced strains with 2x copies of the Rvs genes (2xRVS), 1x copy of each (WT haploid,  
249 1xRVS), 2x copies of the *rvs167 $\Delta$ sh3* gene (2xBAR), or 1 copy of *rvs167 $\Delta$ sh3* gene (1xBAR). Amount of  
250 WT and mutant Rvs167 molecules recruited at endocytic sites varied in these strains between 50  
and 180 copies (Fig5E). Sla1 dynamics remained the same in Rvs duplicated strain (2xRVS) as in the  
251 WT (Fig.6F). In the 2xBAR case, the amount of Rvs167 $\Delta$ sh3 molecules recruited to endocytic sites  
252 increased (Fig.6E), as did Sla1 movement, as well the inward jump of Rvs167 (Fig.6F,G), compared  
253 to 1xBAR. Total Abp1 numbers recruited were reduced in 1xBAR (that is *rvs167 $\Delta$ sh3*), compared to  
254 the 2xBAR, 1xRVS and 2xRVS (Fig5H). Higher Abp1 numbers corresponds to larger Sla1 centroid  
255 movement in both diploid and haploid cells (Fig.6C, D, G, H), suggesting a correlation between the  
256 maximum number of Abp1 recruited and total invagination length.

258 **Discussion**

259 Recruitment and function of the Rvs complex has been studied in this work, and several existing  
260 models for membrane scission have been tested. We propose that Rvs is recruited to endocytic

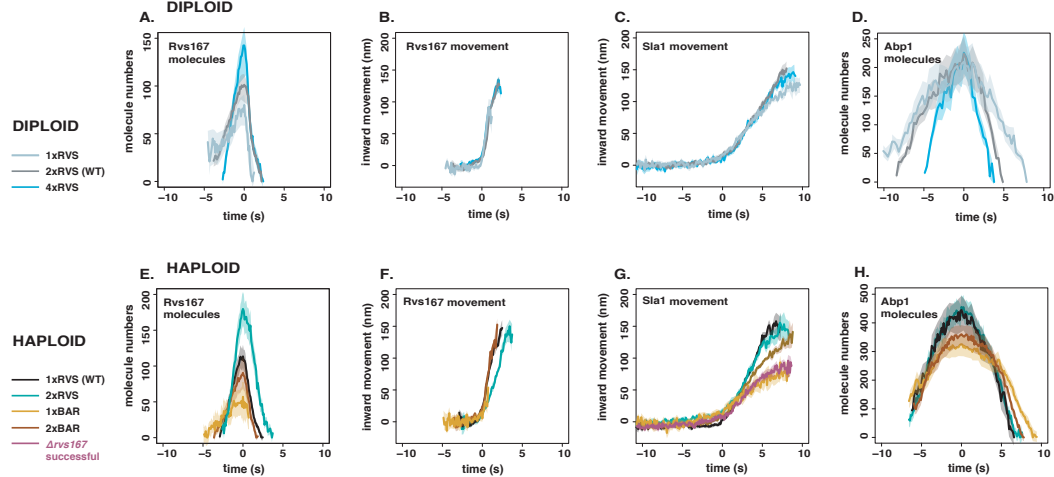


**Figure 6. RVS duplication in haploid and diploid cells** **A:** Recruitment of Rvs167 in diploid strains with different copy number of Rvs167 and Rvs161 genes. **B:** Rvs167 centroid positions in these strains **C:** Sla1 centroid positions in these strains. **D:** Abp1 molecule numbers in same strains, with only one Abp1 allele tagged. **E,F:** Recruitment and centroid positions of Rvs167 and Rvs167 $\Delta sh3$  in haploid strains. **G:** Sla1 centroid positions in these strains. **H:** Abp1 recruitment in the same strains. All centroid positions were aligned in the time axis so that time=0(s) corresponds to beginning of inward movement of each average centroid. Centroids were aligned in the y axis so that y=0(nm) corresponds to the beginning of the average centroid position

261 sites via interactions between the Rvs BAR domains and invaginated membrane, and that SH3  
 262 mediated protein-protein interactions are required for efficient recruitment of Rvs. We found that  
 263 arrival of Rvs at the membrane invagination scaffolds the membrane and prevents membrane  
 264 scission. WT invagination lengths depend on recruitment of a critical number of Rvs molecules.  
 265 Both timing and recruitment efficiency appear crucial to Rvs function.

266 **BAR domains sense *in vivo* membrane curvature and time recruitment of Rvs**  
 267 The curved structure of Endophilin and Amphiphysin BAR dimers ([Peters et al., 2004; Mim et al., 2012](#))  
 268 In the absence of membrane curvature - in *sla2Δ* cells - Rvs167 $\Delta sh3$  domains do not localize  
 269 to endocytic sites (Fig.5B). This demonstrates for the first time that the BAR domain senses and  
 270 requires membrane curvature to localize to endocytic sites. Rvs167 $\Delta sh3$  has a similar average  
 271 lifetime at endocytic sites as full length Rvs167 (Fig.5C,D). However, time alignment with Abp1 shows  
 272 that there is a delay in the recruitment of Rvs167 $\Delta sh3$ , (Fig.5B). Sla1 moves inwards at a slower rate  
 273 in *rvs167Δ sh3* cells, so it takes longer for the membrane in these cells to reach the same invagination  
 274 length as in WT. We propose that Rvs recruitment is timed to specific membrane invagination length-  
 275 therefore to a specific membrane curvature- accounting for the delay in recruitment. The timing of  
 276 recruitment is therefore provided by the BAR domain.

277 **SH3 domains allow efficient and actin independent recruitment**  
 278 Rvs167 $\Delta sh3$  accumulates to about half the WT number (Fig.5C,D), even though the same cyto-  
 279 plasmic concentration is measured (Fig.5 supplement), indicating that loss of the SH3 domain  
 280 decreases the efficiency of recruitment of Rvs. In *sla2Δ* cells, full-length Rvs167 forms patches  
 281 on the membrane (Fig.3B). Since Rvs167 $\Delta sh3$  does not localize to the plasma membrane in *sla2Δ*  
 282 cells, localization of the full-length protein must be mediated by the SH3 domain. That full-length  
 283 Rvs167 is able to assemble and disassemble at cortical patches in *sla2Δ* cells without the curvature-  
 284 dependent interaction of the BAR domain (Fig.3B) indicates that the SH3 domain can mediate  
 285 both the recruitment and disassembly of Rvs at endocytic sites. In *sla2Δ* cells treated with LatA  
 286 (Fig.3B), both membrane curvature and actin-interacting proteins are removed from endocytic sites.

287 Full-length Rvs167 in these cells still shows transient localizations at the plasma membrane: the  
288 SH3 domain is able to localise the Rvs complex in an actin and curvature independent manner.

### 289 **Loss of SH3 domain disrupts endocytic actin network dynamics**

290 In WT cells, the Abp1 and Rvs167 fluorescent intensities reach maxima concomitantly (Fig.5C,D),  
291 and the consequent decay of both coincide. Coincident disassembly indicates that upon vesicle  
292 scission, the actin network is immediately disassembled. Membrane scission occurs around the  
293 intensity peak of the two proteins (*Kukulski et al., 2012; Picco et al., 2015*). This coincident peak is  
294 lost in bar-gpa cells: Rvs167 $\Delta$ sh3 average fluorescent intensity peaks several seconds after Abp1  
295 intensity starts to drop, and the decay of Abp1 is prolonged, taking nearly double the time as in WT.  
296 Although it is not clear what the decoupling of Abp1 and Rvs167 $\Delta$ sh3 peaks means, the changes in  
297 Abp1 dynamics suggests a strong disruption of the actin network dynamics.

### 298 **Rvs acts as a membrane scaffold preventing membrane scission**

299 Invaginations in *rvs167* $\Delta$  cells undergo scission when the Sla1 centroid has moved about 80nm  
300 (Fig.1F), compared to the WT lengths of 140nm. This shows that enough forces are generated at  
301 80nm to cause scission. Since invagination lengths of *rvs167* $\Delta$  cells are increased by overexpression  
302 of the Rvs167 $\Delta$ sh3 domains (Fig.6E-G), we think that localization of Rvs BAR domains to the  
303 membrane tube stabilizes the membrane (*Boucrot et al., 2012; Dmitrieff and Nédélec, 2015*) This  
304 allows the invagination to grow until actin polymerization produces enough forces to sever the  
305 membrane. The requirement for Rvs scaffolding cannot be removed by reducing turgor pressure  
306 (Fig.6supplement? or 7?), so the function of the scaffold is not to counter turgor pressure. There is  
307 a limit to the stabilization by BAR domains: in diploid strains with 4 copies of each RVS gene, the  
308 same amount of actin is recruited before scission. The invaginations lengths are the same as in the  
309 other strains even though more Rvs is recruited. It is possible that the nature of the Rvs complex  
310 interaction with the membrane changes after a certain amount of Rvs is recruited.

311 If enough forces are generated at 80nm, why is scission efficiency decreased in *rvs167* $\Delta$  compared  
312 to WT? Forces from actin may be at a threshold when the invagination is at 80nm. There  
313 could be enough force to sever the membrane, but not enough to sever reliably. The Rvs scaffold  
314 then keeps the network growing to accumulate enough actin to reliably cause scission. Controlling  
315 membrane tube length could also be a way for the cell to control the size of the vesicles formed,  
316 and therefore the amount of cargo packed into the vesicle.

### 317 **What causes membrane scission?**

318 We looked for changes in the dynamics of Sla1 and Rvs167 that would indicate a scission defect  
319 in various mutant strains: longer invaginations than in WT, so Sla1 centroid movements of over  
320 140nm, and a bigger inwards jump of Rvs167 centroid, indicating that a longer invagination has  
321 been cut. In *vps1* $\Delta$  cells, no major changes are seen in Sla1 or Rvs167 dynamics. We conclude that  
322 even if Vps1 is recruited to endocytic sites, it is not necessary for Rvs localization or function, and is  
323 not necessary for scission.

324 In the lipid hydrolysis model, synaptojanins hydrolyze PIP<sub>2</sub> molecules that are not covered by  
325 BAR domains, resulting in a boundary between hydrolyzed and non-hydrolyzed PIP<sub>2</sub>. Interfacial  
326 forces generated at this lipid boundary causes scission (*Liu et al., 2006*). Deleting synaptojanins  
327 Inp51 and Inp52 should increase invagination lengths if scission was driven by lipid hydrolysis.  
328 Sla1 and Rvs centroid dynamics shows that deletion of neither Inp51 nor Inp52 result in scission  
329 delay. In *inp51* $\Delta$  cells, Rvs assembly is slightly slower than that in WT: Inp51 could play a role in  
330 Rvs recruitment. In the *inp52* $\Delta$  strain, about 12% of Sla1-GFP tracks retract, this could suggest  
331 a moderate influence of Inp52 on scission. Rvs centroid persists after scission in *inp52* $\Delta$  cells:  
332 disassembly of Rvs after scission is delayed. Sla1 signal also persists for longer after scission in the  
333 *inp52* $\Delta$  than in WT cells, suggesting that post-scission disassembly of proteins from the vesicle is

334 inhibited in *inp52Δ* cells. Inp52 likely plays a role in recycling endocytic proteins from the vesicle to  
335 the plasma membrane.

336 A protein-friction model has proposed that BAR domains induce a frictional force on the mem-  
337 brane, causing scission (ref!). If more BAR domains were added to the membrane tube at a faster  
338 rate, the frictional force generated as the membrane is pulled under it should increase, and the  
339 membrane should rupture faster. That is, membrane scission should occur as soon as WT forces  
340 are generated on the tube. In Rvs duplicated cells, adding up to 1.6x the WT amount of Rvs at faster  
341 rates to membrane tubes does not affect the length at which the membrane undergoes scission  
342 (Fig.6E). We think that protein friction does not contribute significantly to membrane scission in  
343 yeast endocytosis.

344  
345 We observed that the maximum amount of Abp1 measured in all the diploid strains is about 220  
346 molecules (Fig.6D). Since only one allele of Abp1 is fluorescently tagged in these strains, the total  
347 amount of Abp1 recruited is about  $440 \pm 20$  molecules. In WT haploid cells, the maximum number  
348 of Abp1 measured is  $460 \pm 20$  molecules. We propose that recruitment of a similar amount of Abp1  
349 before scission in all these strains indicates that scission is dependent on the amount of Abp1,  
350 and correspondingly, on the amount of actin recruited. We propose that actin supplies the forces  
351 necessary for membrane scission. The membrane invagination continues until the "right" amount  
352 of actin is recruited. The amount of force necessary is determined by the physical properties of the  
353 membrane like membrane rigidity, tension, and proteins accumulated on the membrane (**Dmitrieff**  
354 and **Nédélec**, 2015). Vesicle scission releases membrane-bound Rvs, resulting in release of the SH3  
355 domains along with BAR domains. Release of the SH3 domains could indicate to the actin network that  
356 vesicle scission has occurred, beginning disassembly of actin components.

### 357 Model for membrane scission

358 We propose that Rvs is recruited to sites by two distinct mechanisms. SH3 domains cluster Rvs at  
359 endocytic sites, increasing the efficiency with which the BAR domains sense curvature on tubular  
360 membranes. BAR domains bind to endocytic sites by sensing tubular membrane. Membrane  
361 shape is stabilized by BAR-membrane interaction against fluctuations that could cause scission.  
362 This prevent actin forces from rupturing the membrane, and the invaginations continue to grow in  
363 length as actin continues to polymerize.

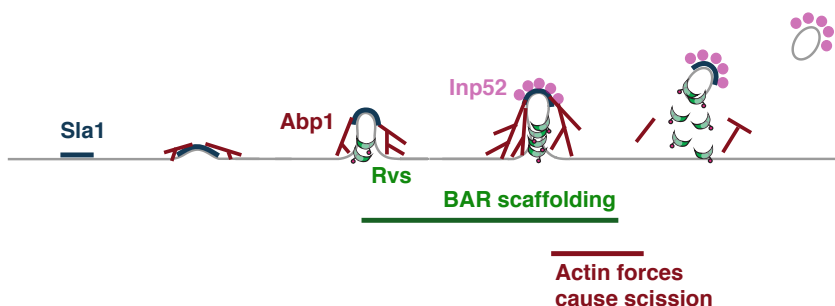


Figure 7. Model for yeast endocytic scission

364 As actin continues to polymerize, enough forces are generated to overcome the resistance to  
365 membrane scission provided by the BAR scaffold. The membrane ruptures, and vesicles are formed.  
366 Synaptojanins may help recruit Rvs at endocytic sites: Inp51 and Inp52 have proline rich regions  
367 that could act as binding sites for Rvs167 SH3 domains. They are involved in vesicle uncoating  
368 post-scission, likely by dephosphorylating PIP<sub>2</sub> and inducing disassembly of PIP<sub>2</sub>-binding endocytic  
369 proteins. Eventually phosphorylation regulation allows endocytic proteins to be reused at endocytic

370 sites, while the vesicle is transported elsewhere into the cell.

### 371 **Methods and Materials**

#### 372 **Homologous recombination with PCR cassette insertion**

373 Tagging or deletion of endogenous genes was done by homologous integration of the product  
374 of a Polymerase Chain Reaction using appropriate primers and a plasmid containing a selection  
375 cassette and fluorescent tag, or only selection cassette for gene deletions. Primers were designed  
376 according to Janke et al, 2004. PCRs used the Velocity Polymerase for fluorescent tagging, and Q5  
377 for gene deletions using the NAT cassette. All fluorescently tagged genes have a C-terminus tag and  
378 are expressed endogenously. Gene deletions and fluorescent tags are checked by PCR. Vps1del and  
379 gene duplications were confirmed by sequencing.

#### 380 **Live-cell imaging and electron microscopy**

##### 381 Sample preparation for live imaging

382 40µL Concanavalin A (ConA) was incubated on a coverslip for 10 minutes. 40µL Yeast cells incubated  
383 overnight at 25C in imaging medium SC-TRP was added to the coverslip after removing the ConA,  
384 and incubated for another 10 minutes. Cells were then removed, adhered cells were washed 3x in  
385 SC-TRP, and 40µL SC-TRP was finally added to the coverslip to prevent cells from drying.

##### 386 Sample preparation for live imaging in LatA and sorbitol treated cells

387 Cells went through the same procedure as above till the last washing step. Instead of SC-TRP, 100x  
388 diluted LatA, or Sorbitol at a final concentration of 0.2M in SC-TRP was added to the adhered cells.  
389 For LatA experiments, cells were incubated in LatA for 10 minutes before imaging. For sorbitol  
390 treatments, cells were imaged within 5 minutes of adding sorbitol.

##### 391 Epifluorescent imaging for centroid tracking

392 Live-cell imaging was performed as in (*Picco et al., 2015*) Picco et al., 2015. All images were obtained  
393 at room temperature using an Olympus IX81 micro- scope equipped with a 100x/NA 1.45 PlanApo  
394 objective , with an additional 1.6x magnification lens and an EMCCD camera. The GFP channel was  
395 imaged using a 470/22 nm band-pass excitation filter and a 520/35 nm band-pass emission filter.  
396 mCherry epifluorescence imaging was carried out using a 556/20 nm band-pass excitation filter and  
397 a 624/40 band-pass emission filter. GFP was excited using a 488 nm solid state laser and mCherry  
398 was excited using a 561 nm solid state laser. Hardware was controlled using Metamorph software.  
399 For single-channel images, 80-120ms was used as exposure time. All dual-channel images were  
400 acquired using 250ms exposure time. Si- multaneouse dual-color images were obtained using a  
401 dichroic mirror, with TetraSpeck beads used to correct for chromatic abberation.

##### 402 Epifluorescent imaging for molecule number quantification

403 Images were acquired as in Picco et al., 2015. Z-stacks of cells containing the GFP-tagged protein  
404 of interest, incubated along with cells containing Nuf2-GFP, were acquired using 400ms exposure  
405 using a mercury vapour lamp, on a CCD camera. Z stacks were spaced at 200nm.

#### 406 **Live-cell image analysis**

407 Images were processed for background noise using a rolling ball radius of 90 pixels. Particle  
408 detection, and tracking was performed for a particle size of 6 pixels, using scripts that com-  
409 bine background subtraction with Particle Tracker and Detector, that can be found on ImageJ  
410 (<http://imagej.nih.gov>). Further analysis for centroid averaging, alignments between dual-color  
411 images and single channel images, for alignment to the reference Abp1 were done using scripts  
412 written in Matlab (Mathworks) and R ([www.r-project.org](http://www.r-project.org)), written originally by Andrea Picco, and  
413 modified by me. Details of analysis can be found at (*Picco et al., 2015*). All movement and intensity  
414 plots from centroid tracking show the average centroid with 95% confidence interval. All molecule

415 number quantifications report either the median or maximum number of molecules with standard  
416 error of mean. Maximum number is preferred over median in cases when the rate of change of  
417 fluorescent intensity of two populations being compared are not similar, and the lifetime of the  
418 protein populations being compared are not similar. The median in this case underreports the  
419 differences in protein accumulation.

#### 420 **Cytoplasmic background quantification**

421 On a maximum intensity projection of time-lapse images, the average pixel intensity within a circle  
422 of set radius in the cytoplasm was measured. This circle is manually arranged so that cortical  
423 patches were excluded, and mean intensity was acquired for about 10 cells of each cell type. A  
424 fixed area outside the cells was drawn, and mean intensity was calculated to establish "background  
425 intensity". This background intensity was then subtracted from the mean intensity to obtain a  
426 rough measure of cytoplasmic intensity. There are some caveats with this quantification: the cells  
427 were not incubated in the same field of view, cellular autofluorescence is assumed to be equal for  
428 the different strains.

#### 429 **Citations**

430 LaTeX formats citations and references automatically using the bibliography records in your .bib  
431 file, which you can edit via the project menu. Use the \cite command for an inline citation, like  
432 ?, and the \citet command for a citation in parentheses (?). The LaTeX template uses a slightly-  
433 modified Vancouver bibliography style. If your manuscript is accepted, the eLife production team  
434 will re-format the references into the final published form. *It is not necessary to attempt to format*  
435 *the reference list yourself to mirror the final published form.* Please also remember to **delete the line**  
436 \nocite{\*} in the template just before \bibliography{...}; otherwise *all* entries from your .bib  
437 file will be listed!

#### 438 **Acknowledgments**

439 Additional information can be given in the template, such as to not include funder information in  
440 the acknowledgments section.

#### 441 **References**

- 442 Bensen, E. S., Costaguta, G., and Payne, G. S. (2000). Synthetic genetic interactions with temperature-sensitive  
443 clathrin in *Saccharomyces cerevisiae*. Roles for synaptojanin-like Lnp53p and dynamin-related Vps1p in  
444 clathrin-dependent protein sorting at the trans-Golgi network. *Genetics*, 154(1):83–97.
- 445 Bitsikas, V., Corrêa, I. R., and Nichols, B. J. (2014). Clathrin-independent pathways do not contribute significantly  
446 to endocytic flux. *eLife*, 3:e03970.
- 447 Boucrot, E., Pick, A., Camdere, G., Liska, N., Evergren, E., McMahon, H. T., and Kozlov, M. M. (2012). Membrane  
448 Fission Is Promoted by Insertion of Amphipathic Helices and Is Restricted by Crescent BAR Domains. *Cell*,  
449 149(1):124–136.
- 450 Bui, H. T., Karren, M. A., Bhar, D., and Shaw, J. M. (2012). A novel motif in the yeast mitochondrial dynamin Dnm1  
451 is essential for adaptor binding and membrane recruitment. *The Journal of cell biology*, 199(4):613–22.
- 452 Cestra, G., Castagnoli, L., Dente, L., Minenkova, O., Petrelli, A., Migone, N., Hoffmüller, U., Schneider-Mergener, J.,  
453 and Cesareni, G. (1999). The SH3 domains of endophilin and amphiphysin bind to the proline-rich region of  
454 synaptojanin 1 at distinct sites that display an unconventional binding specificity. *The Journal of biological  
455 chemistry*, 274(45):32001–7.
- 456 Colwill, K., Field, D., Moore, L., Friesen, J., and Andrews, B. (1999). In Vivo Analysis of the Domains of Yeast Rvs167p  
457 Suggests Rvs167p Function Is Mediated Through Multiple Protein Interactions. *Genetics*, 152(3):881–893.
- 458 D'Hondt, K., Heese-Peck, A., and Riezman, H. (2000). Protein and Lipid Requirements for Endocytosis. *Annual  
459 Review of Genetics*, 34(1):255–295.

- 460 Dmitrieff, S. and Nédélec, F. (2015). Membrane Mechanics of Endocytosis in Cells with Turgor. *PLoS Comput Biol*,  
461 11(10):e1004538.
- 462 Farsad, K., Ringstad, N., Takei, K., Floyd, S. R., Rose, K., and De Camilli, P. (2001). Generation of high curvature  
463 membranes mediated by direct endophilin bilayer interactions. *The Journal of Cell Biology*, 155(2):193–200.
- 464 Ferguson, S. M., Brasnjo, G., Hayashi, M., Wölfel, M., Collesi, C., Giovedi, S., Raimondi, A., Gong, L. W., Ariel, P.,  
465 Paradise, S., O'Toole, E., Flavell, R., Cremona, O., Miesenböck, G., Ryan, T. A., and De Camilli, P. (2007). A selective  
466 activity-dependent requirement for dynamin 1 in synaptic vesicle endocytosis. *Science*, 316(5824):570–574.
- 467 Ferguson, S. M., Raimondi, A., Paradise, S., Shen, H., Mesaki, K., Ferguson, A., Destaing, O., Ko, G., Takasaki, J.,  
468 Cremona, O., O'Toole, E., and De Camilli, P. (2009). Coordinated actions of actin and BAR proteins upstream  
469 of dynamin at endocytic clathrin-coated pits. *Developmental cell*, 17(6):811–822.
- 470 Friesen, H., Humphries, C., Ho, Y., Schub, O., Colwill, K., and Andrews, B. (2006). Characterization of the Yeast  
471 Amphiphysins Rvs161p and Rvs167p Reveals Roles for the Rvs Heterodimer In Vivo. *Molecular Biology of the  
472 Cell*, 17(3):1306–1321.
- 473 Galli, V., Sebastian, R., Moutel, S., Ecard, J., Perez, F., and Roux, A. (2017). Uncoupling of dynamin polymerization  
474 and GTPase activity revealed by the conformation-specific nanobody dynab. *eLife*, 6:e25197.
- 475 Goud Gadila, S. K., Williams, M., Saimani, U., Delgado Cruz, M., Makaraci, P., Woodman, S., Short, J. C., McDermott,  
476 H., and Kim, K. (2017). Yeast dynamin Vps1 associates with clathrin to facilitate vesicular trafficking and  
477 controls Golgi homeostasis. *European Journal of Cell Biology*, 96(2):182–197.
- 478 Grabs, D., Slepnev, V. I., Songyang, Z., David, C., Lynch, M., Cantley, L. C., and De Camilli, P. (1997). The SH3  
479 domain of amphiphysin binds the proline-rich domain of dynamin at a single site that defines a new SH3  
480 binding consensus sequence. *The Journal of biological chemistry*, 272(20):13419–25.
- 481 Grigliatti, T. A., Hall, L., Rosenbluth, R., and Suzuki, D. T. (1973). Temperature-Sensitive Mutations in Drosophila  
482 melanogaster XIV. A Selection of Immobile Adults \*. *Molec. gen. Genet*, 120:107–114.
- 483 Hoepfner, D., van den Berg, M., Philippse, P., Tabak, H. F., and Hettema, E. H. (2001). A role for Vps1p, actin, and  
484 the Myo2p motor in peroxisome abundance and inheritance in *< i>Saccharomyces cerevisiae</i>*. *The Journal  
485 of Cell Biology*, 155(6):979–990.
- 486 Kaksonen, M. and Roux, A. (2018). Mechanisms of clathrin-mediated endocytosis.
- 487 Kaksonen, M., Sun, Y., and Drubin, D. G. (2003). A pathway for association of receptors, adaptors, and actin  
488 during endocytic internalization. *Cell*, 115(4):475–487.
- 489 Kaksonen, M., Toret, C. P., and Drubin, D. G. (2005). A modular design for the clathrin- and actin-mediated  
490 endocytosis machinery. *Cell*, 123(2):305–320.
- 491 Kishimoto, T., Sun, Y., Buser, C., Liu, J., Michelot, A., and Drubin, D. G. (2011). Determinants of endocytic  
492 membrane geometry, stability, and scission. *Proceedings of the National Academy of Sciences of the United  
493 States of America*, 108(44):E979–E988.
- 494 Kübler, E., Riezman, H., Riezman, H., and Riezman, H. (1993). Actin and fimbrin are required for the internalization  
495 step of endocytosis in yeast. *The EMBO journal*, 12(7):2855–62.
- 496 Kukulski, W., Schorb, M., Kaksonen, M., and Briggs, J. G. (2012). Plasma Membrane Reshaping during Endocytosis  
497 Is Revealed by Time-Resolved Electron Tomography. *Cell*, 150(3):508–520.
- 498 Lila, T. and Drubin, D. G. (1997). Evidence for physical and functional interactions among two *Saccharomyces  
499 cerevisiae* SH3 domain proteins, an adenylyl cyclase-associated protein and the actin cytoskeleton. *Molecular  
500 Biology of the Cell*, 8(2):367–385.
- 501 Liu, J., Kaksonen, M., Drubin, D. G., and Oster, G. (2006). Endocytic vesicle scission by lipid phase boundary  
502 forces. *Proceedings of the National Academy of Sciences of the United States of America*, 103(27):10277–82.
- 503 Liu, J., Sun, Y., Drubin, D. G., and Oster, G. F. (2009). The Mechanochemistry of Endocytosis. *PLoS Biol*,  
504 7(9):e1000204.
- 505 Madania, A., Dumoulin, P., Grava, S., Kitamoto, H., Scharer-Brodbeck, C., Soulard, A., Moreau, V., and Winsor,  
506 B. (1999). The *Saccharomyces cerevisiae* Homologue of Human Wiskott-Aldrich Syndrome Protein Las17p  
507 Interacts with the Arp2/3 Complex. *Molecular Biology of the Cell*, 10(10):3521–3538.

- 508 Meinecke, M., Boucrot, E., Camdere, G., Hon, W.-C., Mittal, R., and McMahon, H. T. (2013). Cooperative recruitment  
509 of dynamin and BIN/amphiphysin/Rvs (BAR) domain-containing proteins leads to GTP-dependent membrane  
510 scission. *The Journal of biological chemistry*, 288(9):6651–61.
- 511 Mim, C., Cui, H., Gawronski-Salerno, J. A., Frost, A., Lyman, E., Voth, G. A., and Unger, V. M. (2012). Structural  
512 basis of membrane bending by the N-BAR protein endophilin. *Cell*, 149(1):137–145.
- 513 Moustaq, L., Smaczynska-de Rooij, I. I., Palmer, S. E., Marklew, C. J., and Ayscough, K. R. (2016). Insights into  
514 dynamin-associated disorders through analysis of equivalent mutations in the yeast dynamin Vps1. *Microbial  
515 cell (Graz, Austria)*, 3(4):147–158.
- 516 Munn, A. L., Stevenson, B. J., Geli, M. I., and Riezman, H. (1995). end5, end6, and end7: Mutations that cause  
517 actin delocalization and block the internalization step of endocytosis in *Saccharomyces cerevisiae*. *Molecular  
518 Biology of the Cell*, 6(12):1721–1742.
- 519 Nannapaneni, S., Wang, D., Jain, S., Schroeder, B., Highfill, C., Reustle, L., Pittsley, D., Maysent, A., Moulder, S.,  
520 McDowell, R., and Kim, K. (2010). The yeast dynamin-like protein Vps1:vps1 mutations perturb the internal-  
521 ization and the motility of endocytic vesicles and endosomes via disorganization of the actin cytoskeleton.  
522 *European Journal of Cell Biology*, 89(7):499–508.
- 523 Peters, C., Baars, T. L., Bühler, S., and Mayer, A. (2004). Mutual control of membrane fission and fusion proteins.  
524 *Cell*, 119(5):667–78.
- 525 Picco, A., Mund, M., Ries, J., Nédélec, F., and Kaksonen, M. (2015). Visualizing the functional architecture of the  
526 endocytic machinery. *eLife*, page e04535.
- 527 Rooij, I. I. S.-d., Allwood, E. G., Aghamohammadzadeh, S., Hettema, E. H., Goldberg, M. W., and Ayscough,  
528 K. R. (2010). A role for the dynamin-like protein Vps1 during endocytosis in yeast. *Journal of Cell Science*,  
529 123(20):3496–3506.
- 530 Rothman, J. H., Raymond, C. K., Gilbert, T., O'Hara, P. J., and Stevens, T. H. (1990). A putative GTP binding protein  
531 homologous to interferon-inducible Mx proteins performs an essential function in yeast protein sorting. *Cell*,  
532 61(6):1063–1074.
- 533 Rothman, J. I. and Stevens, T. H. (1986). Protein Sorting in Yeast: Mutants Defective in Vacuole Biogenesis  
534 Mislocalize Vacuolar Proteins into the Late Secretory Pathway. Technical report.
- 535 Shupliakov, O., Löw, P., Grabs, D., Gad, H., Chen, H., David, C., Takei, K., De Camilli, P., and Brodin, L. (1997).  
536 Synaptic vesicle endocytosis impaired by disruption of dynamin-SH3 domain interactions. *Science (New York,  
537 N.Y.)*, 276(5310):259–63.
- 538 Simunovic, M., Manneville, J.-B., Renard, H.-F. O., Johannes, L., Bassereau, P., Callan, A., Correspondence, J.,  
539 Evergren, E., Raghunathan, K., Bhatia, D., Kenworthy, A. K., Voth, G. A., Prost, J., McMahon, H. T., and Callan-  
540 Jones, A. (2017). Friction Mediates Scission of Tubular Membranes Scaffolded by BAR Proteins. *Cell*, 170:1–13.
- 541 Sivadon, P., Crouzet, M., and Aigle, M. (1997). Functional assessment of the yeast Rvs161 and Rvs167 protein  
542 domains. *FEBS letters*, 417(1):21–27.
- 543 Skruzny, M., Brach, T., Ciuffa, R., Rybina, S., Wachsmuth, M., and Kaksonen, M. (2012). Molecular basis for  
544 coupling the plasma membrane to the actin cytoskeleton during clathrin-mediated endocytosis. *Proceedings  
545 of the National Academy of Sciences of the United States of America*, 109(38):E2533–42.
- 546 Smaczynska-de Rooij, I. I., Allwood, E. G., Mishra, R., Booth, W. I., Aghamohammadzadeh, S., Goldberg, M. W., and  
547 Ayscough, K. R. (2012). Yeast Dynamin Vps1 and Amphiphysin Rvs167 Function Together During Endocytosis.  
548 *Traffic*, 13(2):317–328.
- 549 Sweitzer, S. M. and Hinshaw, J. E. (1998). Dynamin Undergoes a GTP-Dependent Conformational Change Causing  
550 Vesiculation. *Cell*, 93(6):1021–1029.
- 551 Takei, K., McPherson, P. S., Schmid, S. L., and Camilli, P. D. (1995). Tubular membrane invaginations coated by  
552 dynamin rings are induced by GTP-γS in nerve terminals. *Nature*, 374(6518):186–190.
- 553 Youn, J.-Y., Friesen, H., Kishimoto, T., Henne, W. M., Kurat, C. F., Ye, W., Ceccarelli, D. F., Sicheri, F., Kohlwein, S. D.,  
554 McMahon, H. T., and Andrews, B. J. (2010). Dissecting BAR Domain Function in the Yeast Amphiphysins Rvs161  
555 and Rvs167 during Endocytosis. *Molecular Biology of the Cell*, 21(17):3054–3069.

- 556 Yu, X. and Cai, M. (2004). The yeast dynamin-related GTPase Vps1p functions in the organization of the actin  
557 cytoskeleton via interaction with Sla1p. *Journal of Cell Science*, 117(17):3839–3853.
- 558 Zhang, P. and Hinshaw, J. E. (2001). Three-dimensional reconstruction of dynamin in the constricted state. *Nature  
559 Cell Biology*, 3(10):922–926.
- 560 Zhao, W.-D., Hamid, E., Shin, W., Wen, P. J., Krystofiak, E. S., Villarreal, S. A., Chiang, H.-C., Kachar, B., and Wu, L.-G.  
561 (2016). Hemi-fused structure mediates and controls fusion and fission in live cells. *Nature*, 534(7608):548–52.
- 562
- 563

## 564 Supplementary Material

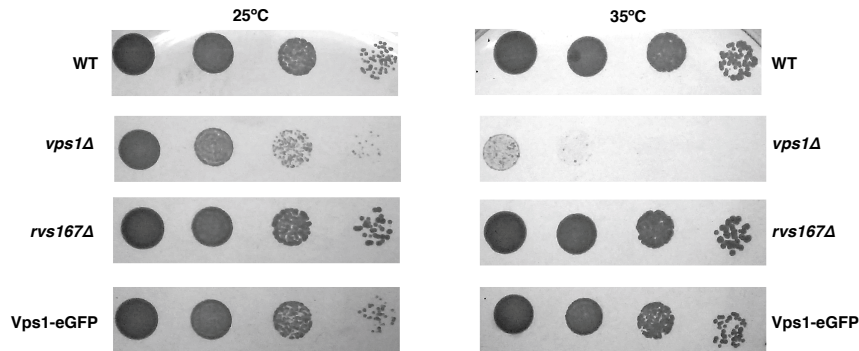


**Figure S1. Growth assay of WT, *vps1Δ*, *rvs167Δ*, and cells expressing Vps1-eGFP at 25°C and 35°C**

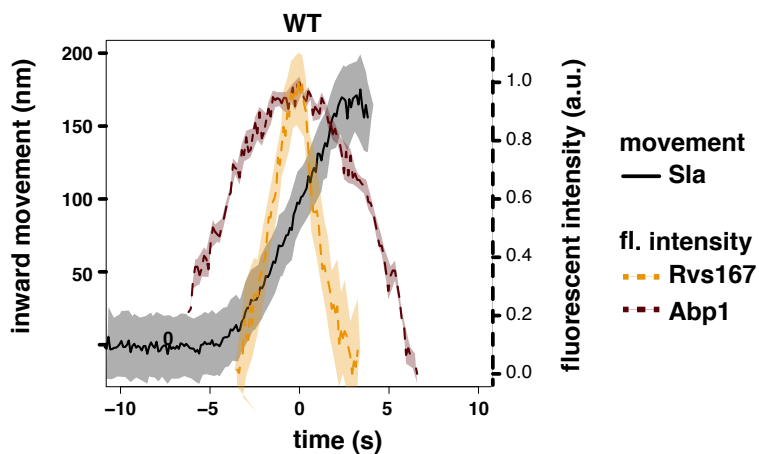


**Figure S2. Sla1 centroid aligned so that time=0(s) is the maximum of Abp1 fluorescent intensity in WT cells (Picco et al., 2015), normalized Abp1 and Rvs167 fluorescent intensities in WT cells**

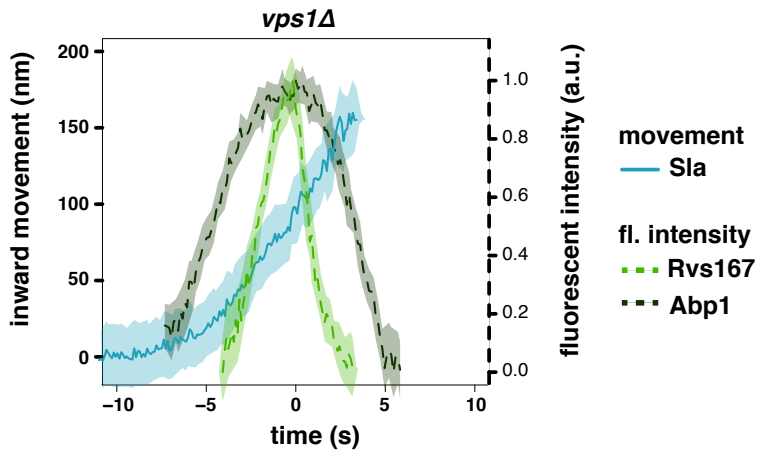


Figure S3. Sla1 centroid aligned so that time=0(s) is the maximum of Abp1 fluorescent intensity in *vps1 $\Delta$*  cells (Picco et al., 2015), normalized Abp1 and Rvs167 fluorescent intensities in *vps1 $\Delta$*  cells

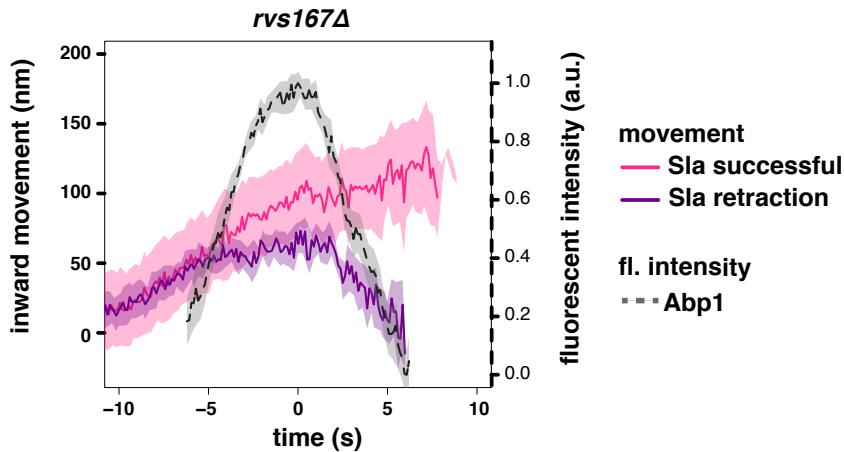


Figure S4. Sla1 centroid aligned so that time=0(s) is the maximum of Abp1 fluorescent intensity in *rvs167 $\Delta$*  cells (Picco et al., 2015), normalized Abp1 fluorescent intensity in *rvs167 $\Delta$*  cells

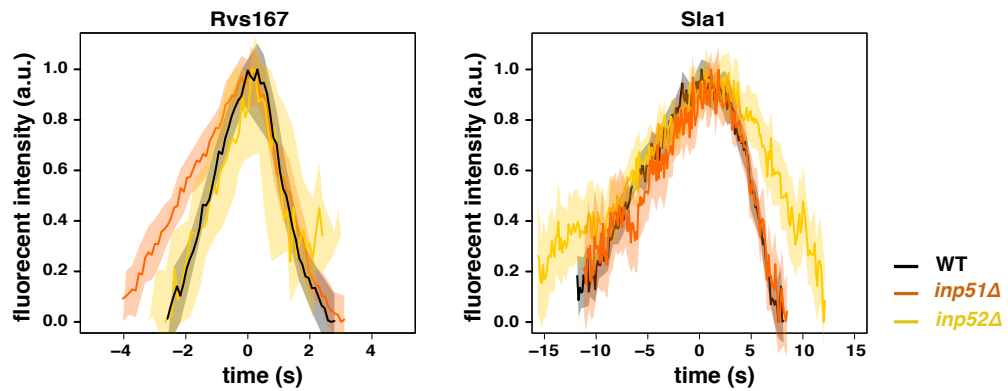
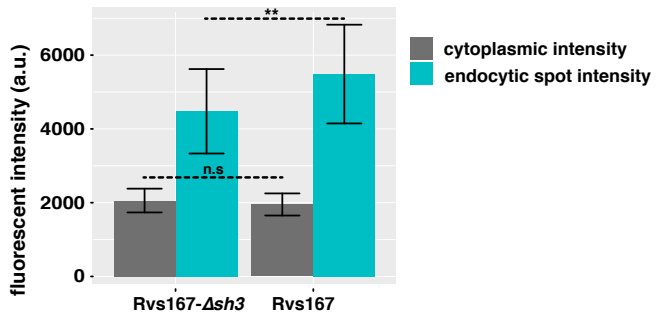


Figure S5. Normalized Rvs167 and Sla1 fluorescent intensities aligned in time so that time=0(s) is the maximum of each corresponding fluorescent intensity profile



**Figure S6. Cytoplasmic intensity and intensity of endocytic patches of Rvs167 and Rvs167 $\Delta sh3$  in WT and rvs167 $\Delta sh3$  cells.** Error bars are standard deviation, p values from t-test, \*= p ≤ 0.05, \*\*= p ≤ 0.01, \*\*\*=p≤0.001.